

True Limits to Precision via Unique Quantum Probe

Sergey Knysh,^{1,2,*} Edward H. Chen,^{3,†} and Gabriel A. Durkin^{1,2,‡}

¹Quantum Artificial Intelligence Laboratory (QuAIL), NASA Ames Research Center, Moffett Field, California 94035, USA

²SGT Inc., 7701 Greenbelt Rd, Suite 400, Greenbelt, Maryland 20770, USA

³Department of Electrical Engineering and Computer Science, Massachusetts Institute of Technology (MIT), Cambridge, Massachusetts 02139, USA

(Dated: November 3, 2018)

Quantum instruments derived from composite systems allow greater measurement precision than their classical counterparts due to coherences maintained between N components; spins, atoms or photons. Decoherence that plagues real-world devices can be particle loss, or thermal excitation and relaxation, or dephasing due to external noise sources (and also due to prior parameter uncertainty). All these adversely affect precision estimation of time, phase or frequency. By a novel technique we uncover the uniquely optimal probe states of the N ‘qubits’ alongside new tight bounds on precision under local and collective mechanisms of these noise types above. For large quantum ensembles where numerical techniques fail, the problem reduces by analogy to finding the ground state of a 1-D particle in a potential well; the shape of the well is dictated by the type and strength of decoherence. The formalism is applied to prototypical Mach-Zehnder and Ramsey interferometers to discover the ultimate performance of real-world instruments.

PACS numbers: 42.50.-p, 42.50.St, 06.20.Dk

Decoherence in quantum systems is responsible for a transition to classical behavior. It degrades the advantage offered by quantum correlations for metrology, specifically the task of parameter estimation.

An overview of the field of quantum metrology is provided in refs. 1,2 and fig.1 outlines the prototypical quantum metrological process, illustrated in parallel for a Mach-Zehnder interferometer and atomic clock. Previously, some of us derived optimal states and metrological bounds for phase estimation subject to particle loss³. Refs. 4,5 additionally derive some bounds for types of individual decoherence following ideas introduced by Fujiwara and Imai⁶. Subsequent work⁷ employs the same approach to tackle collective dephasing. These results are variational in nature and guarantee neither tightness of the bounds, nor provide any intuition about those probe states attaining best precision. Numerical work by Genoni et al.⁸ considers collective dephasing and obtains optimal continuous variable states, restricted to those possessing a Gaussian characteristic function.

We consider for the first time in quantum metrology a very general physical model of decoherence that includes processes of dephasing, relaxation, and excitation. These three categories are investigated via collective or individual mechanisms; an ensemble of N particles is coupled either to a single common bath, or each to its own. For interferometry we explore relevant processes of photon loss combined with collective dephasing, as might occur due to thermal motion of optical components or intrinsic laser noise.

We will show via a new operator formalism, presented in the Methods section, that for a large number of qubits N the problem of identifying the unique and *previously unknown* optimal states in line with tight precision bounds is mapped onto that of finding the ground state of a quantum-mechanical particle in a 1-D potential. Results are presented in table II.

We improve known precision bounds for individual relaxation by a factor of two. It is also revealed that for collective dephasing the ‘quantum’ component of error (in excess

	Collective ($\dot{\Gamma}^\sigma \times$)	Individual ($\dot{\gamma}^\sigma \times$)
Dephasing: $\sigma \mapsto 0$	$S^z \rho S^z - \frac{1}{2} \{ (S^z)^2, \rho \}$	$\sum_k s_k^z \rho s_k^z - \frac{N}{4} \rho$
Relaxation: $\sigma \mapsto -$	$S^- \rho S^+ - \frac{1}{2} \{ S^+ S^-, \rho \}$	$\sum_k (s_k^- \rho s_k^+ - \frac{1}{2} \{ s_k^+ s_k^-, \rho \})$
Excitation: $\sigma \mapsto +$	$S^+ \rho S^- - \frac{1}{2} \{ S^- S^+, \rho \}$	$\sum_k (s_k^+ \rho s_k^- - \frac{1}{2} \{ s_k^- s_k^+, \rho \})$

TABLE I: **Lindblad operators for various types of noise**, $\mathcal{L}_\sigma[\rho]$ are summarized in this table. Entries are multiplied by appropriate rates of either collective ($\dot{\Gamma}^0, \dot{\Gamma}^-, \dot{\Gamma}^+$) or individual ($\dot{\gamma}^0, \dot{\gamma}^-, \dot{\gamma}^+$) dephasing, relaxation or excitation, respectively. Overdots denote derivatives $\partial/\partial\theta$ with respect to ‘time-like’ phase variable θ .

of classical diffusion) turns out to be 10 times (π^2) larger than suggested by previous reports⁷.

Ultimately, all bounds we derive are achievable *as they are constructive*; obtained via the discovery of a probe state that is uniquely optimal in the large ensemble limit $N \gg 1$. The asymptotic tightness of our bounds then follows naturally. The general form of this probe may be fairly exotic, but despite this, in many typical, combined noise regimes the optimal probes approach a Gaussian profile (albeit with mean and variance set by the ‘flavor’ of decoherence). This is pertinent when it comes to the challenge of generating these probes in the laboratory. For mixed noise types the predicted optimal states can be apparent for modest ensembles of $N \lesssim 30$ particles, indicating the power of this analytic approach whether the available resources are few or many. See fig.4 for a comparison with numerics.

Finally, by fixing the total resources νN , where ν is the number of measurement trials and N is the size of each multi-qubit ‘cluster’ (subjected independently to the system dynamics), we uncover novel scaling laws in table II. For individual decoherence there exist entangled states with particular structure that is most robust to noise; it is always the largest qubit

clusters with this structure that offer the best precision. Collective decoherence, by contrast, is eventually deleterious to *all* entangled states. Beyond a critical cluster size N_c overall performance decreases. At the critical size, clusters of NOON⁹ states – despite their recent reputation for fragility to decoherence¹⁰ – are resurrected as an optimal metrology resource.

Phase Estimation with Decoherence

The precision of parameter estimation is controlled by three factors: (i) the input state or probe $|\psi\rangle$ subjected to (ii) dynamical evolution which imprints the parameter θ to be estimated, and (iii) the specific measurement choice that reveals details of the evolved state and therefore the parameter, see fig.1. A fourth, often overlooked aspect is the need to combine many repeated measurement outcomes into a minimum-variance, unbiased estimator. Classical Fisher Information (CFI) gives a measure of precision for such an efficient estimator without choosing the estimator explicitly. Quantum Fisher Information (QFI) then represents CFI optimized over all possible measurements^{11,12}. The only remaining step in deriving the ultimate bounds (for fixed system dynamics) is optimization over the probe state using QFI as a precision metric. This is our task in the present work.

Dynamical evolution of an ensemble of N qubits can be described by a master equation¹³:

$$\frac{d\rho}{d\theta} = -i[S^z, \rho] + \underbrace{\sum_{\sigma} \mathcal{L}_{\sigma}[\rho]}_{\text{noise terms}}, \quad (1)$$

where unitary shift operator $S^z = \sum_{k=1}^N s_k^z$ conserves total spin $S \leq N/2$: the eigen-equation is $S^z|S, m\rangle = m|S, m\rangle$. The largest, $S = N/2$ space is completely symmetric under particle exchange; for bosons (e.g. photons) this is the only possibility. This spin formalism is applicable to ensemble of atoms in a double-well potential¹⁶, optical interferometers¹⁷, or Ramsey interferometry used in atomic clocks¹⁸ (see fig. 1).

Absent noise, minimum variance of phase estimation is inversely proportional to the variance of phase shift operator S^z :

$$\nu \text{ var } \theta_{\text{est}} = 1/F, \quad F = 4 \text{ var } S^z, \quad (2)$$

where ν is the number of independent measurements. Optimal probe states inhabit the subspace of largest $S = N/2$. They have $\langle S, \pm S|\psi\rangle = \psi_{\pm S} = 1/\sqrt{2}$ as the only non-zero amplitudes: a celebrated ‘GHZ’¹⁹ aka ‘NOON’⁹ probe state. Also note that, as $\text{var } \theta_{\text{est}} = 1/(\nu N^2)$, it becomes advantageous to utilize the largest ensembles possible, trading off the number of measurements for larger N when the total qubit resources νN are constrained.

The situation certainly becomes more complex when any decoherence effects are included. An initially pure state decays into a mixture due to coupling to the environment, which can be modeled by adding Lindblad terms within eq.(1) (summarized in table I). We are careful to distinguish individual

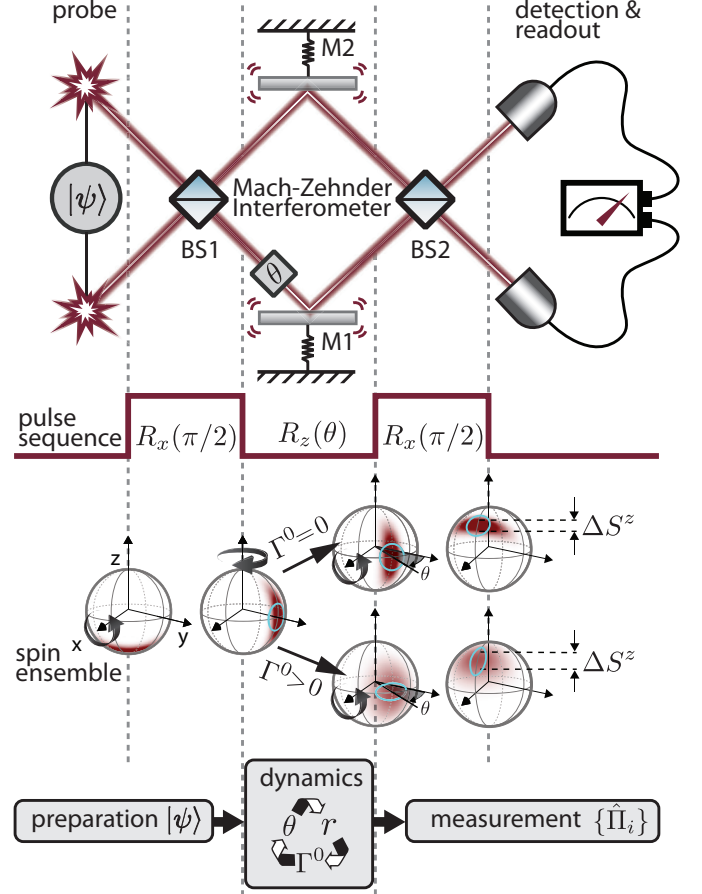


FIG. 1: **Quantum phase estimation** is illustrated for optical (Mach-Zehnder) and atomic (Ramsey) interferometry. Process diagram beneath indicates three physical steps of quantum metrology: probe state preparation, dynamical evolution, and measurement. Not shown is the final statistical analysis of measurement results to produce a parameter estimation. The Schwinger isomorphism maps accumulation of relative phase θ due to interferometer path difference to temporal evolution of N two-level atoms or spins for time θ , i.e. free rotation $R_z(\theta)$. Actions of beam splitters BS1, BS2 are equivalent to $\pi/2$ -pulses producing rotations about x -axis. Red density plots on spin spheres depict probability (Husimi¹⁴) distributions for $N = 60$ phase-squeezed state of eqn.(5). For comparison, blue circles indicate the boundary of probability distribution for the spin-coherent ‘pointer’ state, for which all 60 spins are aligned. Increased projection measurement error ΔS^z due to dephasing $\Gamma^0 = 0.05$ is indicated in the lower branch (S^z measurement may be performed by photon-counting in both Mach-Zehnder arms after BS2, or S^x measurement between BS1 and BS2.). Dephasing may occur at interferometer mirrors M1, M2 by thermal motion or radiation pressure. Other sources of noise include photon loss r .

and collective decoherence. The former would be appropriate when each qubit is coupled to its own bath, while the latter results in much stronger noise when all qubits share common bath and have the same coupling constant. A consideration of weak decoherence involves the effect of phase diffusion alone; characteristic ensemble dephasing time $T_2^* \propto 1/\dot{\Gamma}^0$ is much less than the characteristic relaxation time $T_1 \propto 1/\dot{\Gamma}^-$.

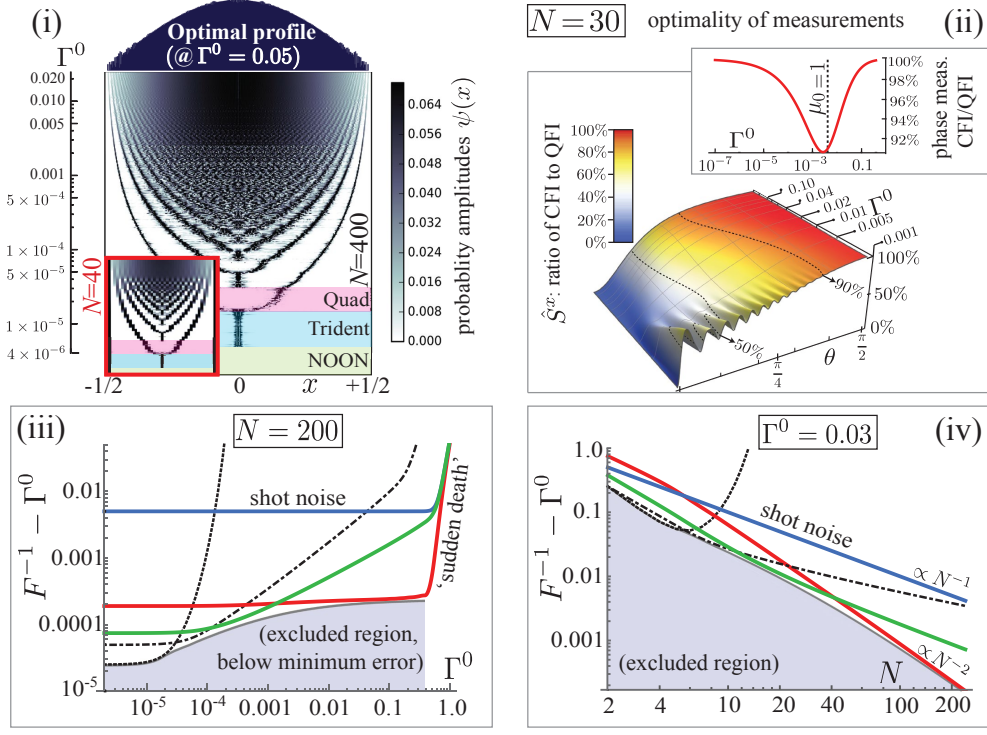


FIG. 2: **Collective Dephasing has an associated optimal state** that evolves via a characteristic ‘Menorah’ structure in (i) for $N = 400$ (inset for $N = 40$) as dephasing increases (in the vertical direction). Each horizontal row of pixels ($x = m/N$) correspond to the array of optimal state components ψ_m for $m \in [-N/2, +N/2]$ found by numerical search; each component’s amplitude indicated by pixel brightness. As dephasing increases a third component appears at $m = 0$ in addition to the two extremal ($m = \pm N/2$) NOON components to make a ‘Trident’ optimal state. That central component in turn bifurcates symmetrically at the next critical point to make a ‘Quad’ state; those two new components diverge towards the boundary. By such a series of accelerating bifurcations the optimal state eventually form a continuous Cosine profile, eq. (5), slightly ragged but already apparent at $\Gamma^0 = 0.05$ (upper barchart). Figure (ii) gives optimality (ratio of CFI to QFI) of phase measurements (2D line plot) and S^x or photon counting (3D surface) for the state of eq.(5) and $N = 30$. Phase measurements exhibit a dip, they are optimal for both large and small mass $\mu_0 = \Gamma^0 N^2$, but not for intermediate regime $\mu_0 \approx 1$. For S^x measurements efficiency depends on the phase neighborhood as well as dephasing Γ^0 . Biasing the interferometer phases $\theta \approx \pi/2$ allows such measurements to be close to optimal for all Γ^0 . Plots (iii) and (iv) show quantum measurement error, from eq.(6), for different families of states. The asymptotically optimal Cosine state (red curve) is compared with phase states³⁰ (green) with $\psi_m = 1/\sqrt{N+1}$ and Holland-Burnett states³³ (black chained line) with $\psi_m = d_{m,0}^S(\pi/2)$ (note. 34). NOON states (black dotted) gain advantage for very small dephasing $\Gamma^0 \lesssim 10^{-5}$. A spin-coherent state [blue curve, $\psi_m = d_{m,S}^S(\pi/2)$] is operating at the shot-noise limit exactly, $1/N$. Note the ‘sudden death’ of precision as $\Gamma^0 \gtrsim 1$, when the density matrix is nearly diagonal and symmetric under shift by S^z . The phase-squeezed state (5) is already dominant for moderately small $N \gtrsim 40$ in (iv) and across three orders of magnitude of Γ^0 in (iii). Lowest possible quantum error is found numerically; indicated by the upper boundary of the ‘excluded’ region.

Many realistic scenarios will involve stronger relaxation, and we shall consider this too. Excitation will be included for completeness, playing a role at finite temperatures. It should be emphasized that this is a fairly exhaustive list of decoherence processes. For instance, depolarization considered in refs. 4,6,15 is not a distinct process but can be described as a combination of dephasing, relaxation and excitation e.g. with $\gamma^0/2 = \gamma^- = \gamma^+$.

In the present work we eschew *ad hoc* precision bounds in favor of analysis of dynamics in the limit $N \gg 1$ where the major gains of quantum metrology may be realized, if phase error is shown to scale with some negative power of N . The optimal state may be approximated by a wavefunction $\langle N/2, m | \psi \rangle \mapsto \psi(x)/\sqrt{N}$ [where $x = m/N$ is taken

to be continuous] corresponding to the ground state of a second order differential equation akin to the time-independent Schrödinger equation (see Methods section). Following the analogy, the ground state ‘energy’ eigenvalue λ_{\min} determines the minimum attainable phase variance:

$$-\psi''_{\text{opt}} + \mu(x)\psi_{\text{opt}} = \lambda_{\min}\psi_{\text{opt}}, \quad \text{var } \theta_{\text{est}} \geq \lambda_{\min}/(\nu N^2). \quad (3)$$

The form of the potential well $\mu(x)$ depends on the flavor and strength of decoherence, see results of table II. It should also include infinite walls $\mu(x) = +\infty$ for $|x| > 1/2$ to ensure that the wavefunction vanishes outside the interval: $-N/2 \leq m \leq N/2$.

We have corroborated our results with numerical study, pre-

sented in figures: 2, 3, 4. As seen in fig.2(i) and fig.4, the characteristic asymptotic behavior will often ‘set in’ for relatively small particle number $10 < N < 100$, allaying concerns that these results are of interest only in the limit of very large ensembles. To contrast, if we had naïvely chosen to optimize precision bounds appearing elsewhere in the literature^{5,7}, we would recover NOON-like ‘optimal’ probes having only a few discrete components (states that actually perform poorly in noisy conditions), rather than the necessary continuous profile.

Collective Dephasing

In the following sections we describe various noise combinations in more detail, but let’s begin with the simplest scenario, that of ‘pure’ collective dephasing. It is the dominant noise in atom and spin ensembles, where energy and particle number are conserved²⁰. It occurs in light beams due to laser noise, optical path length fluctuations²¹ and radiation pressure at the surface of mirrors^{7,22}. It plays a role in optic-fiber interferometric sensors²³ where thermal perturbations and mechanical strains can lead to measurable diffusion in both interferometric phase and polarisation of light. Collective dephasing is the prevalent noise for ions confined to traps²⁴.

Dephasing presents an exponential suppression of the off-diagonal elements of the density matrix. Equivalently it can be viewed as random fluctuations of the phase θ itself with amplitude $\sqrt{\Gamma^0}$:

$$\rho = \int_{-\infty}^{\infty} |\psi(\theta)\rangle\langle\psi(\theta)| \frac{e^{-(\theta-\bar{\theta})^2/2\Gamma^0}}{\sqrt{2\pi\Gamma^0}} d\theta. \quad (4)$$

The density matrix is a mixture of pure states $|\psi\rangle$, each evolved by a different phase θ , but the ensemble is Gaussian-distributed with mean $\bar{\theta}$ and variance Γ^0 . The statistical ensemble may form via independent measurements on many identical pure states, or may result simply from coupling to the environment. Overall, environmental dephasing is indistinguishable from an acknowledgment of initial phase uncertainty, even when noise is absent, indicating the ubiquity and central role of collective dephasing in the estimation process.

The quantum contribution to phase error under dephasing is a subtle, second-order ($\propto 1/N^2$) correction to the classical phase noise. Attempts to find optimal states by WKB approximation were defeated and the solution required careful application of a novel operator approach, presented in Methods. (We identify the dephasing channel with an imaginary-time Feynman propagator for a free particle.) Further details of the calculation can be found in Appendix A. We find that the optimal state and minimum variance are described by eqn. (3) with a ‘flat’ potential $\mu(x) = \mu_0 = N^2\Gamma^0$ between the infinite walls at $x = \pm 1/2$. Let us call this large parameter ‘mass’. A semiclassical asymptotic expansion of QFI maybe carried out in powers of $1/\mu_0$; truncating the series after the first few non-trivial terms is the basis of many of our results. For large ‘mass’ $\mu_0 \gg 1$, the optimal state is given by the ground state of a ‘particle in a box’, a *phase-squeezed* Cosine function spanning half a period. Expressed in terms of

discrete amplitudes,

$$|\psi_{\text{opt}}\rangle = \sqrt{\frac{2}{N+1}} \sum_{m=-N/2}^{N/2} \cos \frac{\pi m}{N+1} \left| \frac{N}{2}, m \right\rangle. \quad (5)$$

(This state was originally proposed in ref. 25 as a candidate for precision in the absence of noise.) Phase error approaches $\nu N^2 \text{var } \theta_{\text{est}} = \mu_0 + \pi^2$ in the limit of large N . Additionally, we constrain ourselves to a scenario where $\Gamma^0 \ll 1$; large values severely suppress phase-carrying off-diagonal elements of the density matrix. We shall see also that entangled ensembles offer no advantages when noise exceeds certain threshold $\Gamma_c^0 \lesssim 1$.

Convergence of the optimal probe from a discrete NOON state to the continuous phase-squeezed profile above is observed numerically in fig.2 (i), progressing by a sequence of accelerating bifurcations as dephasing increases. Fig. 2.(iii) and (iv) give quantitative comparison with families of states proposed in the literature.

A way to generate the optimal phase-squeezed state was presented by Combes and Wiseman²⁶. The state is generated by the action of a counter-twisting spin-squeezing Hamiltonian $S^y S^z + S^z S^y$ (ref. 27) on an unentangled spin-coherent state. An exotic physical mechanism was given by Andre and Lukin involving interaction between atoms via polaritons²⁸. Yet another approach utilizes the dynamics of a two-mode Bose-Einstein condensate for optimal phase squeezing²⁹.

Combining Errors from Classical Noise and Measurement

An optimal state (5) can be found by minimizing the functional for the reciprocal of QFI (see the Methods),

$$\nu \text{var } \theta_{\text{est}} = \frac{1}{F} \approx \Gamma^0 + \frac{1}{N^2} \int \psi'^2(x) dx, \quad (6)$$

valid in the ‘large-mass’ regime $\mu_0 \gg 1$. Notice that to this lowest order the phase uncertainty is a sum of errors added in quadrature; the amplitude Γ^0 is the variance of a classical random phase noise or equivalently that of a (Gaussian) prior uncertainty, recall eqn.(4). The second term is the quantum measurement uncertainty, as follows:

In this large mass regime canonical phase measurements, i.e. projections onto the (over-complete) basis of phase states $|\theta\rangle = \frac{1}{\sqrt{N+1}} \sum_m e^{-im\theta} \left| \frac{N}{2}, m \right\rangle$, are optimal³¹; they produce a classical Fisher information equal to the QFI. Because phase states are non-orthogonal they produce a finite-width distribution of measurement error; the phase distribution of the probe must be *convolved* with the classical phase uncertainty of width $\sqrt{\Gamma^0}$ from eq.(4) when dephasing (or prior uncertainty) is present. The convolution of two Gaussians produces another with variance equal to the sum of the two components variances. Hence Gaussian profile probe states (with a Gaussian-distributed phase distribution) produce (6) exactly. Such is the spin-coherent state obtained in fig.1 between the beam-splitters when a photon-number state enters

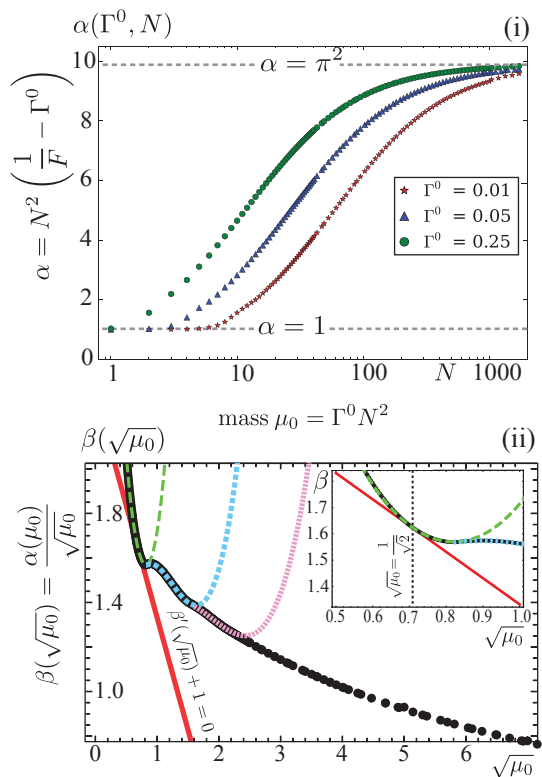


FIG. 3: **Numerical Results** for collective dephasing. In (i) individual plot points correspond to numerical searches for the minimum coefficient α of the measurement error contribution α/N^2 to mean-squared phase error. Red stars, blue triangle and green circles are for dephasing $\Gamma^0 \mapsto \{0.01, 0.05, 0.25\}$, respectively. Coefficient α interpolates from unity to π^2 [from the bounds of eq.(7)] as universal ‘mass’ parameter $\mu_0 = \Gamma^0 N^2$ increases. In graph (ii) previous numerical data collapses onto a single curve—indicating dependency on a single combined parameter, $\mu_0 = \Gamma^0 N^2$ (black points). The α value for optimal clustering is located where function $\beta(\sqrt{\mu_0})$ has gradient $= -1$, corresponding to $\mu_0 = 1/2$ (inset, vertical dotted line). The β function is plotted for NOON (green), ‘Trident’ (light-blue) and ‘Quad’ states (pink), indicating that optimal clusters will be NOON states. (See discussion in the Methods.) The minima of these analytic curves correspond to the bifurcation points in the Menorah of fig.2(i).

just one port of the first beamsplitter. The quantum measurement mean-squared error for this state is $1/N$ [see fig.2 (iv)]; poor ‘shot-noise’ scaling can be explained by vacuum fluctuations leaking into the other ‘dark’ port³².

For generic probes, (6) may still be applied when Gaussian-distributed ‘classical’ phase fluctuations are the dominant error source. In this scenario, to maximize precision and QFI one must minimize the phase variance of the quantum measurement component in (6), since Γ^0 is fixed. The state to minimize phase measurement error (in the absence of noise²⁵) is (5), hence its appearance above (and its description as a ‘phase-squeezed’ state). Optimality of this state is inevitable for increasing dephasing *or* ensemble size N , as the relevant universal parameter is the product $\mu_0 = \Gamma^0 N^2$.

In the opposite ‘small-mass’ regime $\mu_0 \ll 1$, the

GHZ/NOON state achieves the best precision – as in the noiseless scenario. The mean squared quantum error component is $1/N^2$ or about 10 times smaller than that achieved with the ‘minimum phase variance’ (phase-squeezed) state (5). It is a subtle point that this reduction is possible by a more efficient estimator than the sample mean, (that was only sufficient for $\mu \gg 1$ because the final phase distribution was approximately Gaussian). Interestingly, canonical phase measurements are optimal in both small and large mass regimes but not in the intermediate regime $\mu_0 \approx 1$; observe the dip of fig.2(ii).

We must add that such measurements are not a unique choice: projections onto eigenstates of S^x can also saturate these bounds in the limits of either small or large mass μ_0 . Examine the surface plot of fig.2 (ii) indicating performance of S^x measurements as a function of both phase and dephasing. Because canonical phase measurements are much more difficult to implement,³⁵ it is significant that S^x measurements can be optimal— they correspond to photon counting in interferometry or ensemble ‘population difference’ measurement in an atom clock .

In the intermediate-mass regime, minimum error interpolates between two bounds

$$\Gamma^0 + 1/N^2 \leq 1/F \leq \frac{\Gamma^0 + \pi^2/N^2}{[1 - \pi\tilde{p}(\pi)]^2}; \quad (7)$$

optimal phase estimation requires coordination of a highly non-trivial probe state, measurement, and estimator statistic. The first inequality can be understood as a Fisher information inequality for the sum of two random variables: $F_{x+y}^{-1} \geq F_x^{-1} + F_y^{-1}$ (where x and y are respectively the true interferometric phase and the random fluctuating phase), appearing previously in ref. 7. The upper bound on $1/F$ above has been modified via a denominator that takes phase periodicity into account³⁶. [Here $\tilde{p}(\theta)$ is the probability distribution obtained by convolving the distribution of random phase from eq.(4) and phase measurement error, given explicitly in Appendix A, eq.(34)]. The effect of this denominator can be ignored in the limit of small dephasing, but leads to error increasing in proportion to $\exp(\Gamma^0)$ as soon as $\Gamma^0 \gtrsim 1$, a ‘sudden death’ of precision. See fig.2(iii).

Clustering and Shot-Noise Scaling

For a fixed *total* number of resources νN , increasing N is done at the expense of the number of independent measurements ν , increasing the variance due to classical phase diffusion limit Γ^0/ν . The ‘quantum’ component of error decreases owing to Heisenberg scaling N^{-2} . Optimal cluster size N_c is determined by a tradeoff between these contributions. The minimum phase estimation variance for this optimal choice becomes $c\sqrt{\Gamma}/(\nu N)$ in the limit of small Γ^0 . The value of the prefactor can be bounded between 2 and 2π by performing independent optimizations of on both sides of double inequality (7). Obtaining the precise value requires the knowledge of the functional dependence of $\alpha(\mu_0)$ of the prefactor of quantum component of error α/N^2 since optimal cluster size N_c necessarily corresponds to the intermediate mass $\mu \sim 1$. We

find (in fig.3) that $c = \sqrt{2}e$, corresponding to $N_c = 1/\sqrt{2\Gamma^0}$ ('mass' $\mu_0 = 1/2$). A NOON state is still the optimal choice of probe at this mass value. The unexpected 'resurrection' of NOON state as the optimal probe needs more explanation. While it is true that NOON states are extremely fragile in the presence of decoherence,¹⁰ collective dephasing degrades the performance of *all* states with large N . For decoherence of individual character, precision always improves for increasing N but requires employing exotic probes that are more robust to noise than NOON states. With collective dephasing, the only strategy to cope with noise is to refrain from using large ensembles $N \gtrsim N_c \sim 1/\sqrt{\Gamma^0}$. And for large dephasing, entangled states may offer no benefits at all. By comparing the exact QFI expressions for a spin $S = 1$ system and two unentangled $S = 1/2$ particles, $2 \exp(-\Gamma^0)$, there is a critical dephasing $\Gamma_c^0 \approx 0.251$ beyond which sending N particles one at a time is better than using entangled clusters (even bipartite). By similar comparisons, tripartite ($S = 3/2$) and 4-part ($S = 2$) clusters become superior for $\Gamma^0 < 0.081$ and $\Gamma^0 < 0.041$, respectively.

Interplay of Dephasing, Relaxation and Excitation

For most combinations of Γ^σ for $\sigma \mapsto \{0, +, -\}$, there will exist a wide range of magnitudes of N where the optimal state is determined by solving Schrödinger-type equation (3) in a new, curved 'potential', (see the Methods). Relaxation and excitation processes give rise to an additional contribution $N^2(\Gamma^- + \Gamma^+)x^2/(1/4 - x^2)$ to the potential (see table II). As Γ^\pm increases, the optimal state interpolates between the Cosine state for pure dephasing and a state centered at the origin with a Gaussian profile of width $1/[2(\Gamma^- + \Gamma^+)^{1/4}\sqrt{N}]$. The quantum component of error is $\sqrt{\Gamma^- + \Gamma^+}/N$, i.e. it exhibits shot-noise scaling. The next order term is of order $1/N^2$, due to anharmonic corrections to the potential; it plays a role in determining the optimal cluster size N_c .

This result holds only for $N \lesssim 1/\Gamma^\mp$. For larger ensembles the dynamics predict a 'super-sudden death' of precision. Error increases as $\exp[N(\Gamma^- - \Gamma^+)/2]$, an effect related to Dicke's superradiance³⁷: Coherent emission of quanta into a shared bath results in much stronger dissipation.

Addressing the issue of optimal clustering, our findings are unchanged from the case of collective dephasing. NOON states are robust with respect to relaxation and excitation, except when $N \gtrsim 1/\Gamma^\pm$ where *all* states perform poorly. On the other hand, degradation of performance due to dephasing will occur as $N \gtrsim 1/\sqrt{\Gamma^0}$, prior to 'super-sudden death' of precision in the regime where all decoherence processes have comparable strength. Minimum phase estimation variance is primarily determined by the strength of dephasing with only a small correction due to other processes, see table II.

Individual Decoherence

Let's now consider a model where each qubit is coupled to its own bath,^{38,39} rather than a single common bath.

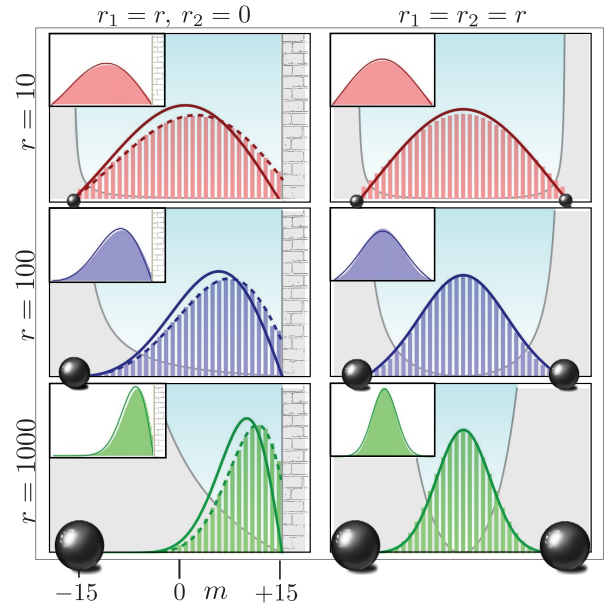


FIG. 4: **Dephasing and particle loss – Comparing analytics and numerics** in an interferometer for $N = 30$ (inset $N = 100$) and $\Gamma^0 = 0.25$; optimal state components are shown by solid bars. The left column is for losses in the sample arm only, $r_2 = 0$, and the right column for symmetric loss, $r_1 = r_2$. Increasing loss parameter $r \mapsto 10, 100, 1000$ for $N = 30$ corresponds to reduced transmittivities = 75%, 23%, 3%. Analytical solutions ψ are superimposed as continuous line plots – the ground state of a particle in a 1-D potential well (gray shaded region). This well is created by two repulsive Coulomb point sources, of 'charge' $\propto r$. If $r_2 = 0$ the second Coulomb source is replaced by an infinite wall. The ground-state in that case is given by a Whittaker function with imaginary arguments $\psi(y, \eta) \propto y e^{-iy/2} {}_1M_1(1 - i\eta, 2; iy)$ [note 41] with $y = \lambda(1 + 2m/N)$ and $\eta = r/8\lambda$. Boundary conditions to uniquely specify ψ in $N \sim \infty$ limit requires setting it to zero at Coulomb sources and the base of the wall. For finite N we can treat the Whittaker function as a 'variational ansatz' rather than an analytic result, and optimize over the single parameter λ (dashed curves), relaxing the 'wall' boundary condition. For larger N the node quickly converges on the point $m/N = x = 1/2$ and the exact solution is recovered – compare the inset $N = 100$ data. In the large N limit there can be no non-zero amplitude at the boundary – Any discontinuity in $\psi(x)$ at $x = 1/2$ causes an anomalous spike in kinetic energy $\propto \psi'(x)^2$, raising the solution out of the ground state of eq.(3). In the symmetric-loss case the optimal state converges to a Gaussian profile of width $= (2r^{1/4})^{-1}$ when loss is the dominant decoherence, $r \gg \mu_0$.

We are primarily interested in a regime where the strength of decoherence remains constant while the number of qubits grows large. A somewhat surprising result (see the Methods) is that the ultimate precision and the optimal state depend on the total strength of decoherence $\gamma = \gamma^0 + \gamma^- + \gamma^+$ but not on fractions attributed to particular processes: dephasing, excitation, and relaxation. The form of potential $\mu(x)$ is given in table II. Its minimum determines an asymptotically tight upper bound:

$$\text{var } \theta_{\text{est}} \geq \frac{e^\gamma - 1}{\nu N}. \quad (8)$$

	Collective Decoherence		Individual Decoherence	Hybrid (Interferometry)
Decoherence Process	Dephasing Only (Γ^0)	General Case (Γ^0, Γ^\pm)	General Case (γ^0, γ^\pm)	Collective Dephasing, Loss ($\Gamma^0, \gamma_1, \gamma_2$)
Universal Parameters	$\mu_0 = N^2\Gamma^0$	μ_0 , and $\mu_1 = N^2(\Gamma^+ + \Gamma^-)$	$r = N [e^{\gamma^0 + \gamma^- + \gamma^+} - 1]$	$\mu_0, r_{1,2} = N [e^{\gamma_{1,2}} - 1] \equiv 4N\epsilon_{1,2}^2$
Potential $\mu(x)$ for $N \gg 1$ (shape)	$\begin{cases} \mu_0 & -\frac{1}{2} < x < \frac{1}{2} \\ \infty & x \geq \frac{1}{2} \end{cases}$ (box)	$\mu_0 + \mu_1 \frac{x^2}{1/4 - x^2}$	$\frac{r}{1 - 4x^2}$ (Coulomb-symmetric)	$\mu_0 + \frac{1}{4} \left(\frac{r_1}{1/2 + x} + \frac{r_2}{1/2 - x} \right)$ (Coulomb)
ψ_{opt} profile: {center, width, shape}	{0, ≈ 0.21 , Cosine}	{0, $(2\mu_1^{1/4})^{-1}$, Gaussian}	{0, $(2r^{1/4})^{-1}$, Gaussian}	{ $\frac{\sqrt{r_1 - \sqrt{r_2}}}{2(\sqrt{r_1} + \sqrt{r_2})}$, $\frac{(r_1 r_2)^{1/8}}{\sqrt{r_1 + \sqrt{r_2}}}$, Gaussian*}
Gives m.s.e. lower bound (for conditions)	$\Gamma^0 + \frac{\pi^2}{N^2}$ ($\mu_0 \gg 1$)	$\Gamma^0 + \frac{\sqrt{\Gamma^- + \Gamma^+}}{N}$ ($\mu_0 \gg \sqrt{1 + \frac{\mu_1}{\mu_0}}$ and $N \ll 1/\Gamma^\pm$)	$\frac{\exp(\gamma^0 + \gamma^- + \gamma^+) - 1}{N}$ ($r \gg 1$)	$\Gamma^0 + \frac{(\epsilon_1 + \epsilon_2)^2}{4N}$ ($r_{1,2} \gg 1$)
Optimal clustering bound ($N = N_c$)		$\frac{\sqrt{2e\Gamma^0}}{N}$	n/a	$\frac{(\epsilon_1 + \epsilon_2)^2}{N} + \begin{cases} \frac{4}{N} \left(\frac{a_1}{4} \right)^{\frac{4}{3}} \epsilon_1 (\Gamma^0)^{\frac{1}{4}} \\ \frac{3}{2^{2/3}} \frac{(\epsilon_1 + \epsilon_2)^{\frac{4}{3}} (\Gamma^0)^{\frac{1}{3}}}{N (\epsilon_1 \epsilon_2)^{1/3}} \end{cases}$

TABLE II: **Quantum Precision Limits:** Summary of main results derived in this paper. Widths of optimal states are rescaled for variable $x = m/N \in [-1/2, 1/2]$; multiply by N for original scaling. The optimal state for interferometry is marked Gaussian* as it has a Gaussian profile when $r_{1,2} \gg 1$; however when $r_2 = 0$ and $\mu_0 \gg 1$ the profile approximates an Airy-type profile³ at large r_1 . The last two rows show mean-squared error lower bounds on $\nu\theta_{\text{est}}$ for ν independent measurements; the final row has been optimized for a large fixed *total* number of resources νN . Note that for individual decoherence there is no optimal clustering N_c for a fixed νN as performance always increases monotonically with N . In interferometry, the Airy/Gaussian shape of the optimal profile in the large loss limit gives a modified phase error for fixed νN . This proceeds via next-to-leading order contributions to the potential $\mu(x)$ – resulting phase error is shown in the final table element for both single mode, $\epsilon_2 = 0$ (upper) and two-mode loss cases, $\epsilon_2 > 0$ (lower). Constant $a_1 \approx -2.33$ is the first zero of the Airy function.

Approximating the potential by a parabola we find the optimal state and the leading order correction $2\sqrt{r}/(\nu N^2) = O(\frac{1}{\nu N^{3/2}})$. Bound (8) coincides with the bound obtained earlier for pure dephasing^{4,5} but is *stronger* than all known bounds for relaxation and depolarization (*ibid*).

Application to Interferometry

In a two-mode interferometer, collective dephasing takes place concurrently with particle loss, in effect a hybridized individual/collective noise. Photons are easily lost in optical components but atoms may also be absorbed into the surrounding thermal cloud during the decay of a Bose-Einstein condensate⁴⁰.

Lindblad operators $\hat{\gamma}_k(a_k \rho a_k^\dagger - \frac{1}{2}\{a_k^\dagger a_k, \rho\})$, with $k = 1, 2$ represents losses in sample and reference arms respectively with rates $\hat{\gamma}_{1,2}$. (In fig.1 these are the modes with mirrors $M1$ and $M2$ respectively.) Here a_k, a_k^\dagger are particle annihilation and creation operators. Beamsplitters with transmission $e^{-\gamma_1}$ and $e^{-\gamma_2}$ couple particles (photons) into environmental modes to describe loss. This may be chiefly due to absorption in the phase sample, while noise in the reference arm is tightly controlled ($\gamma_2 = 0, \Gamma_2^0 = 0$). In gravitational wave detection, closely losses in both arms due to imperfections of mirror surfaces, diffraction, and detector inefficiency are

likely^{42,43}. Fig. 4 illustrates the optimal state for fixed dephasing and increasing values of loss.

The presence of dephasing ultimately forces the optimal state to take a continuous form given by a solution to the Schrödinger equation (3) with potential

$$\mu(x) = \mu_0 + \frac{1}{4} \left(\frac{r_1}{\frac{1}{2} + x} + \frac{r_2}{\frac{1}{2} - x} \right) \quad (9)$$

that corresponds to placing two *repulsive* Coulomb sources at $x = \pm \frac{1}{2}$ (see table II). The second source should be replaced by an infinite wall in the ‘one-mode loss’ scenario. The constant term is $\mu_0 = N^2\Gamma^0$, where $\Gamma^0 = \Gamma_1^0 + \Gamma_2^0$ is the total dephasing.

For large N , the optimal state becomes increasingly localized near the minimum of (9). Table II gives phase estimation error as a sum of classical phase diffusion limit Γ^0 and error attributable to loss. Interestingly, errors attributable to loss in either arm ϵ_1/\sqrt{N} and ϵ_2/\sqrt{N} add in magnitude rather than in quadrature.

A fraction $\frac{\epsilon_1 \epsilon_2}{\epsilon_1^2 - \epsilon_1 \epsilon_2 + \epsilon_2^2}$ of error in excess of Γ^0 in each space of $N_d < N$ total *detected* photons is attributable to ‘loss-induced dephasing’. The *total* number of lost particles can be inferred as $N - N_d$, but we cannot learn how the lost photons were distributed between the two interferometer arms. Doing so would erase all phase information in the measurement, we would have projected onto a S^z eigenstate. This uncertainty

in the distribution of particles presents a *de facto* extra source of dephasing.

Optimal partitioning of total particle resources νN involves interplay between Γ^0 and the corrections phase variance resulting from higher order terms in the potential. (The contribution scaling $\propto 1/(\nu N)$ is unaffected by partitioning since the total νN is fixed.) These corrections produce novel precision bounds and scaling, indicated in the last row of table II, valid when $r_{1,2} \gg 1$.

Determining the structure of the optimal states subject to physical decoherence represents an important advance in metrology, however the physical generation of optimal states is now a new challenge, especially for large N . Elaborate proposals do exist to ‘tailor-make’ the amplitudes ψ_m in optical systems⁴⁴ but it is not clear that these would be scaleable.

On the other hand, we have seen (table II) that in certain noise scenarios the optimal state converges on a Gaussian profile. It has been observed⁴⁵ that Gaussian-profile probe states may be generated naturally in atom interferometers; they approximate the ground state of the hamiltonian $S^x - \beta(S^z)^2$. They also occur through the action of a single-axis twisting Hamiltonian on a coherent state. These may represent feasible techniques by which the optimal probes might be realized.

By learning (i) the ultimate resource/performance trade-off, (ii) the unique form of the associated optimal probes and (iii) possible ways to generate those probes, we are taking three positive steps towards optimal design of next-generation quantum sensors subject to realistic decoherence.

Methods

Computing Quantum Fisher Information

Pure dephasing leads to exponential suppression of off-diagonal matrix elements

$$\rho(x, x') = \psi(x) \exp\{-N^2 \Gamma^0 (x - x')^2 / 2\} \psi(x'), \quad (10)$$

where we may view $x = m/N$ as a continuous variable for large N and small dephasing Γ^0 . The Gaussian kernel is a (imaginary time) Feynman propagator e^{-T} for a free particle with mass $\mu = N^2 \Gamma^0$. Writing amplitudes as $e^{-V/2}$ with ‘potential’ $V = -\ln \psi^2(x)$, an operator diagonal in coordinate representation, we may write (10) as a thermal state e^{-H} of an abstract Hamiltonian H . Now H is expressible by a series of commutators of V and T via a Baker-Campbell-Hausdorff (BCH) identity.⁴⁶ (More explicit details in Appendix A.)

We apply this novel representation for the Quantum Fisher Information, valid for an arbitrary unitary shift parameter ($\partial \rho / \partial \theta = -i[U, \rho]$),

$$F = \langle [U, 2 \tanh(\frac{1}{2}[H, \bullet])U] \rangle, \quad (11)$$

as a series of nested commutators, following the power series expansion of the hyperbolic tangent. Here $[H, \bullet] \equiv \text{ad}_H$ represents the adjoint endomorphism of Lie algebra: $[H, \bullet]U = [H, U]$ and $[H, \bullet]^2 U = [H, [H, U]]$ and so on. Angular brackets represent taking a trace with the density matrix.

Nested commutators in the BCH identity⁴⁶ and the expansion (11) form a series in powers of $1/\mu$:

$$\frac{F}{N^2} = \frac{1}{\mu_0} - \frac{1}{\mu_0^2} \int \psi'^2 dx + O\left(\frac{1}{\mu_0^3}\right) \quad (12)$$

retaining the two leading terms and using $U = S^z$ for phase evolution. In the limit $\mu_0 \gg 1$ this can be rewritten in the more intuitive form of eqn. (6).

In the more general scenario, when other types of noise are included, the strength of exponential suppression of phase-carrying elements of the density

matrix varies along the diagonal: $\exp[-\frac{1}{2}\mu(\frac{x+x'}{2})(x-x')^2]$. Additional suppression $\propto V''(\frac{x+x'}{2})$ results from gradient $\psi'(x)$.

QFI is then given approximately by

$$\frac{F}{N^2} \approx \int \frac{\psi^2}{\mu(x) + \frac{1}{4}V''} dx \approx \int \left[\frac{\psi^2}{\mu(x)} - \frac{\psi'^2}{\mu^2(x)} \right] dx, \quad (13)$$

where in the latter expression we drop corrections to the coefficient of $\psi^2(x)$ of orders $O(\frac{1}{\mu^2})$ and higher (resulting from integration by parts). This new ‘Lagrangian’-type formulation of QFI is generally applicable to any probe state having characteristic length scale (e.g. width) much larger than $1/\sqrt{\mu}$, a small parameter.

The Euler-Lagrange equation for the variational maximum of (13) reduces to ‘Schrödinger’ equation (3) at the same approximation level: we use the fact that $\sqrt{\langle \mu^2(x) \rangle - \langle \mu(x) \rangle^2} \ll \mu(x)$ [here angular brackets denote integration with $\psi_{\text{opt}}^2(x)$ corresponding to the ground state of ‘Schrödinger equation’].

General Decoherence Model

Collective decoherence in the most general setting can be described by master equation

$$\frac{d\rho}{dt} = \frac{\partial \rho}{\partial \theta} + \dot{\Gamma}^0 \frac{\partial \rho}{\partial \Gamma^0} + \dot{\Gamma}^- \frac{\partial \rho}{\partial \Gamma^-} + \dot{\Gamma}^+ \frac{\partial \rho}{\partial \Gamma^+}, \quad (14)$$

where the first term represents unitary phase evolution $\partial \rho / \partial \theta = -i[S^z, \rho]$ and $\dot{\Gamma}^0, \dot{\Gamma}^-, \dot{\Gamma}^+$ are the rates of collective dephasing, relaxation and excitation, respectively. Individual processes, e.g. relaxation, are described by

$$\begin{aligned} \frac{\partial \rho_{mm'}}{\partial \Gamma^-} &= f_{m+1} f_{m'+1} \rho_{m+1 m'+1} - f_m f_{m'} \rho_{mm'} \\ &\quad - \frac{1}{2} (f_m - f_{m'})^2 \rho_{mm'}, \end{aligned} \quad (15)$$

with $f_m = \sqrt{(S-m)(S+m+1)}$.

The first two terms on the right hand side describe probability-conserving drift and diffusion along the diagonal $m - m' = \text{const}$. Their effects can be ignored as long $N\Gamma^- \ll 1$. The last ‘absorption’ term suppresses off diagonal elements with exponent that is proportional to $(m - m')^2$ for not too large distance from the diagonal. Thus relaxation represents as additional dephasing process, of strength that varies along the main diagonal: $N^2 \Gamma^- \frac{x^2}{1/4 - x^2}$. The effects of pure dephasing, relaxation and thermal excitation are combined in a single ‘potential’ $\mu(x)$, presented in table II.

Individual decoherence does not conserve total spin but the density matrix factorizes into independent sectors labeled by $S \leq \frac{N}{2}$. Detailed analysis presented in Appendix A shows that the master equation can similarly be viewed as a combination of drift and diffusion, albeit in two dimensional space with $x = m/N$ and $y = S/N$ as well as induced dephasing of variable rate

$$\dot{\mu} = N \frac{\dot{\gamma}}{4(y^2 - x^2)} \quad (\text{where } \dot{\gamma} = \dot{\gamma}^0 + \dot{\gamma}^- + \dot{\gamma}^+), \quad (16)$$

which must be integrated along the path $(x(\theta), y(\theta))$. Variable x in QFI functional (13) represents $x(\theta)$ at the end of the evolution so that a change of variables would be required to write it in terms of the original probe state $\psi(x)$. Equivalently, it can be applied verbatim if x is taken to mean $x(0)$ at the beginning of the evolution.

When integrating the dephasing rate, drift alone may be taken into account; diffusion results in negligible correction. Using expression for the drift (v_x, v_y) we observe that

$$\frac{d}{d\theta}(y^2 - x^2) \equiv 2y v_y - 2x v_x = -\dot{\gamma}(y^2 - x^2), \quad (17)$$

which is easily integrated. Further integration of the dephasing rate $\dot{\mu}$ starting from point (x, y) at $\theta = 0$ produces the ‘potential’ $\mu(x)$:

$$\mu(x) = \frac{N(e^\gamma - 1)}{4(y^2 - x^2)}. \quad (18)$$

As expected, minimum error is obtained when the probe state corresponds to $S = N/2$.

Particle loss is described by the following terms in master equation:

$$\frac{\partial \rho_{mm'}^{(S)}}{\partial \gamma_{1,2}} = f_{S+\frac{1}{2}}^{\pm} m \pm \frac{1}{2} f_{S+\frac{1}{2}}^{\pm} m' \pm \frac{1}{2} \rho_{m \pm \frac{1}{2} m' \pm \frac{1}{2}}^{(S+\frac{1}{2})} - f_{Sm}^{\pm} f_{Sm'}^{\pm} \rho_{mm'}^{(S)} - \frac{1}{2} (f_{Sm}^{\pm} - f_{Sm'}^{\pm})^2 \rho_{mm'}^{(S)} \quad (19)$$

with $f_{Sm}^{\pm} = \sqrt{S \pm m}$ and γ_1, γ_2 denoting losses in sample and reference arms respectively.

As before, we introduce continuous variables $x = m/N$ and $y = S/N$. The last term in eqn. (19) is the rate of induced dephasing which in the continuous limit approaches $\dot{\mu} = \frac{N}{4} (\frac{\dot{\gamma}_1}{y+x} + \frac{\dot{\gamma}_2}{y-x})$. This must be integrated along the path that solves continuous equations for the drift, $\frac{d}{d\theta}(y \pm x) = -\dot{\gamma}_{1,2}(y \pm x)$. Adding a contribution $\mu_0 = N^2 \Gamma^0$ due to collective dephasing we obtain the ‘potential’ of eqn. (9) in the main text.

Optimal Clustering for Collective Dephasing

Interpolating between upper/lower bounds of eq.(7), the error in the intermediate regime is

$$\text{var}\theta_{\text{est}} = \frac{\Gamma^0}{\nu} + \frac{\alpha(\mu_0)}{\nu N^2} \quad (20)$$

where numerical coefficient $\alpha \in [1, \pi^2]$ is itself a function of mass $\mu_0 = \Gamma^0 N^2$. Rewriting in terms of mass:

$$\text{var}\theta_{\text{est}} = \frac{\sqrt{\Gamma^0}}{\nu N} \left(\sqrt{\mu_0} + \frac{\alpha(\mu_0)}{\sqrt{\mu_0}} \right) \quad (21)$$

Now if we choose to fix our resources νN we can differentiate the bracketed expression with respect to mass to find the minimum $\text{var}\theta_{\text{est}}$. This gives $2\mu_0 \alpha'(\mu_0) - \alpha(\mu_0) + \mu_0 = 0$, or equivalently $\beta'(\sqrt{\mu_0}) + 1 = 0$ for $\beta(\sqrt{\mu_0}) = \alpha(\mu_0)/\sqrt{\mu_0}$. Recasting numerical data for minimum quantum error in the presence of dephasing (generated for multiple N and Γ^0 values) in terms of $\beta(\sqrt{\mu_0})$ and locating the point at which the gradient = -1 unveils the optimal $\mu_0 = 1/2$, see fig.3. Therefore the optimal cluster size is $N_c = 1/\sqrt{2\Gamma^0}$.

Acknowledgements

GAD acknowledges useful discussions with Roman Schnabel. EHC was supported by the NASA Office of the Chief Technologists Space Technology Research Fellowship under the guidance of Dirk Englund and Vadim Smelyanskiy.

- * Electronic address: Sergey.I.Knysh@nasa.gov
 † Electronic address: ehchen@mit.edu
 ‡ Electronic address: Gabriel.Durkin@qubit.org
¹ V. Giovannetti, S. Lloyd, and L. Maccone, *Science* **306**, 1330 (2004).
² V. Giovannetti, S. Lloyd, and L. Maccone, *Nature Photon.* **5**, 222 (2011).
³ S. Knysh, V. N. Smelyanskiy, and G. A. Durkin, *Phys. Rev. A* **83**, 021804(R) (2011).
⁴ R. Demkowicz-Dobrzanski, J. Kolodynski, and M. Guta, *Nature Comm.* **3**, 1063 (2012).
⁵ B. M. Escher, R. L. de Matos Filho, K. Davidovich, *Nature Physics* **7**, 406 (2011).
⁶ A. Fujiwara and H. Imai, *J. Phys. A* **41**, 255304 (2008).
⁷ B. M. Escher, L. Davidovich, N. Zagury, and R. L. de Matos Filho, *Phys. Rev. Lett.* **109**, 190404 (2012).
⁸ M. G. Genoni, S. Olivares, M. G. A. Paris *Phys. Rev. Lett* **106**, 153603 (2011).
⁹ B. C. Saunders, *Phys. Rev. A* **40**, 24172427 (1989); Dowling, J. P., *Contemporary Physics*, **49** (2), 125-143 (2008).
¹⁰ B. R. Bardhan,, K. Jiang1, and J. P. Dowling, *Phys. Rev. A* **88**, 023857 (2013).
¹¹ S. L. Braunstein and C.M. Caves, *Phys. Rev. Lett.* **72**, 3439 (1994).
¹² M. G. A. Paris, *Int. J. Quant. Inf.* **7**, 125 (2009).
¹³ D.F. Walls and G.J. Milburn, *Quantum Optics*, Springer, Berlin (1996).
¹⁴ J. Ma, X. Wang, C. P. Sun and F. Nori, *Phys. Rep.* **509**, 89-165 (2011).
¹⁵ M. Sasaki, M. Ban, and S. M. Barnett, *Phys. Rev. A* **66**, 022308 (2002).
¹⁶ C. Lee, *Phys. Rev. Lett.* **97**, 150402 (2006).
¹⁷ B. Yurke, S. L. McCall, and J. R. Klauder, *Phys. Rev. A* **33**, 4033 (1986).
¹⁸ S. A. Diddams, J. C. Bergquist, S. R. Jefferts, and C. W. Oates, *Science* **306**, 1318 (2004).
¹⁹ J. J. Bollinger, W. M. Itano, D. J. Wineland, and D. J. Heinzen,

- Phys. Rev. A* **54**, R4649 (1996).
²⁰ Y. C. Liu, G. R. Jin, and L. You, *Phys. Rev. A* **82**, 045601(2010).
²¹ A. Franzen, B. Hage, J. DiGiuglielmo, J. Fiurásek, and R. Schnabel, *Phys. Rev. Lett.* **97**, 150505 (2006).
²² C. M. Caves, *Phys. Rev. Lett.* **45**, 75 (1980).
²³ V. G. M. Annamdas, *Int. J. Mat. Eng.*; **1** (1): 1-16 (2011)
²⁴ T. Monz, P. Schindler, J. T. Barreiro, et al., *Phys. Rev. Lett.* **106**, 130506 (2011).
²⁵ G.S. Summy and D.T. Pegg, *Optics Comm.* **77**, 1. 75-79, (1990); D. W. Berry and H. M. Wiseman, *Phys. Rev. Lett.* **85**, 5098 (2000).
²⁶ J. Combes and H. M. Wiseman *J. Opt. B: Quantum Semiclass. Opt.* **7** 14-21 (2005)
²⁷ M. Kitagawa and M. Ueda, *Phys. Rev. A* **47**, 5138 (1993).
²⁸ A. Andre and M.D. Lukin, *Phys. Rev. A*, **65** 5, 053819 (2002).
²⁹ G. R. Jin, Y. An, T. Yan, and Z. S. Lu, *Phys. Rev. A* **82**, 063622 (2010).
³⁰ A. Vourdas, *Phys. Rev. A* **41**, 1653 (1990).
³¹ See Appendix A.
³² C. M. Caves, *Phys. Rev. D* **23**, 1693 (1981).
³³ M. J. Holland and K. Burnett, *Phys. Rev. Lett* **71**, 1355 (1993).
³⁴ Wigner rotation element $d_{m,m'}^S(\chi) = \langle S, m | \exp\{-i\chi \hat{S}^y\} | S, m' \rangle$.
³⁵ S. M. Barnett, *Philosophical Transactions of the Royal Society of London. Series A: Mathematical, Physical and Engineering Sciences* **355** 1733 (1997): 2279-2290
³⁶ S. M. Barnett and D. T. Pegg, *Phys. Rev. A* **41**, 3427 (1990).
³⁷ R. H. Dicke, *Phys. Rev.* **93**, 99-110 (1954).
³⁸ S. F. Huelga, C. Macchiavello, T. Pellizzari, et al., *Phys. Rev. Lett.* **79**, 3865 (1997).
³⁹ M. Foss-Feig, K. R. A. Hazzard, J J Bollinger, A. M. Rey, and C W Clark, *New J. Phys.* **15** 113008, (2013).
⁴⁰ Yun Li, P. Treutlein, J. Reichel and A. Sinatra, *Euro. Phys. J. B* **68**, 365 (2009); S. Knoop, J. S. Borbely, R. van Rooij, and W. Vassen, *Phys. Rev. A* **85**, 025602 (2012).
⁴¹ This is Kummer confluent hypergeometric function:

- ${}_1M_1(a, b; z) = 1 + \frac{a}{b}z + \frac{a(a+1)}{b(b+1)}\frac{z^2}{2!} + \dots$
- ⁴² J. Abadie, et al., Nature Physics, **7** (12), pp. 962-965, (2011)
- ⁴³ R. Schnabel, N. Mavalvala, D.E. McClelland, and P.K.Lam, Nat. Comm, **1**, 121.
- ⁴⁴ M. Dakna, J. Clausen, L. Knöll, and D.-G. Welsch, Phys. Rev. A **59**, 1658 (1999).

- ⁴⁵ I.Tikhonenkov, M. G. Moore, and A. Vardi Phys. Rev. A **82**, 043624 (2010).
- ⁴⁶ N. Hatano and M. Suzuki, *Finding exponential product formulas of higher orders*. Quantum Annealing and Other Optimization Methods. Springer Berlin, 37-68 (2005).

Appendix A

Semiclassical Expansion of Quantum Fisher Information

Introducing operator representation with

$$V = -\ln \psi^2(x), \quad T = \frac{1}{2} \ln \frac{2\pi}{\mu} + \frac{P^2}{2\mu}, \quad (22)$$

continuous limit of the density matrix following collective dephasing process can be written as

$$\rho = e^{-V/2} e^{-T} e^{-V/2} = e^{-H_0 - H_1 - \dots} \quad (23)$$

where

$$H_0 = T + V, \quad (24)$$

$$H_1 = \frac{1}{12} [T, [T, V]] + \frac{1}{24} [V, [T, V]] = -\frac{\{P, \{P, V''\}\}}{48\mu^2} + \frac{V'^2}{24\mu},$$

etc., are successive terms in the Baker-Cambell-Hausdorff expansion (only odd orders appear for symmetrically-split operators)

Sylvester equation for the symmetric logarithmic derivative of the density matrix undergoing arbitrary unitary evolution may be written as

$$\frac{1}{2} \{e^{-H}, L\} = -i[U, e^{-H}], \quad (25)$$

where we explicitly write the density matrix as a thermal state $\rho = e^{-H}$. Multiplying this by $e^{H/2}$ from both left and right ($e^{H/2} \dots e^{H/2} = e^{H/2} \dots e^{H/2}$) and exploiting the representation of $e^A B e^{-A}$ as

$$\exp([A, \bullet])B \equiv B + [A, B] + \frac{1}{2!} [A, [A, B]] + \dots, \quad (26)$$

we rewrite eqn. (25) in the following form:

$$\cosh\left(\frac{1}{2}[H, \bullet]\right)L = -2i \sinh\left(\frac{1}{2}[H, \bullet]\right)U. \quad (27)$$

Since superoperators on both sides are commuting, both sides can be left-multiplied by $\cosh^{-1}\left(\frac{1}{2}[H, \bullet]\right)$. [Here $\cosh^{-1}x = 1/\cosh x$, not the inverse hyperbolic cosine denoted $\operatorname{arcosh}x$.] Substituting SLD into the expression for the Quantum Fisher Information,

$$F = \operatorname{Tr}(\rho L^2) = \operatorname{Tr}(i[U, L]\rho), \quad (28)$$

eqn. (11) of the main text is reproduced.

Expansion of hyperbolic tangent is performed to third order,

$$F = \langle [U, [H, U]] \rangle - \frac{1}{12} \langle [U, [H, [H, [H, U]]]] \rangle + \dots; \quad (29)$$

using $U = NX$ (where $X \equiv S^z/N$) for phase evolution, leading order contribution to QFI is

$$\frac{F_0}{N^2} = \langle [X, [H_0, X]] \rangle = \frac{1}{\mu}, \quad (30)$$

which represents the classical phase diffusion limit $\nu \operatorname{var} \theta_{\text{est}} = \Gamma^0$. Next order corrections is from third order terms in BCH identity⁴⁶ and the expansion of hyperbolic tangent,

$$\frac{F_1}{N^2} = \langle [X, [H_1, X]] \rangle - \frac{1}{12} \langle [X, [H_0, [H_0, [H_0, X]]]] \rangle = -\left\langle \frac{V'''}{4\mu^2} \right\rangle, \quad (31)$$

which is evaluated using integration by parts and noting boundary conditions $\psi(\pm\frac{1}{2}) = 0$. These two leading terms are presented in eqn. (12); higher-order commutators form a series expansion in powers of $1/\mu$.

Gaussian-profile Probes and Canonical Phase Measurements

When Gaussian-profile states $\psi(x) \propto e^{-Kx^2/4}$ are employed, the algebra has finite basis: X^2 and P^2 . Closed form expression for 'Hamiltonian' is

$$H = \frac{1}{2} \ln \frac{K}{\mu_0} + \operatorname{arsinh} \sqrt{\frac{K}{4\mu_0}} \times \left[\sqrt{K(\mu_0 + \frac{K}{4})} X^2 + \frac{P^2}{\sqrt{K(\mu_0 + \frac{K}{4})}} \right]. \quad (32)$$

For the symmetric logarithmic derivative and QFI we obtain, respectively,

$$\frac{L}{N} = -i \frac{P}{\mu_0 + K/4}, \quad \frac{F}{N^2} = \frac{1}{\mu_0 + K/4}, \quad (33)$$

verifying that (6) is exact.

That the SLD is diagonal in P -representation suggests that the optimal measurement corresponds to projection onto eigenstates e^{iPX} . For finite N , it must be replaced by a POVM built from overcomplete set of phase states $|\theta\rangle = \sum_m \exp(-im\theta)|S, m\rangle$, so-called 'canonical' phase measurement. For general symmetric pure probe state $[\psi^*(x) = \psi(-x)]$, these measurement saturate QFI bound¹¹ and result in phase-independent distribution of error. For the Cosine probe state of eqn. (5),

$$p(\delta\theta) = \frac{4}{(N+1)\pi} \left(\frac{\sin \frac{\pi}{N+1} \cos \frac{\delta\theta}{2} \cos \frac{\delta\theta}{N+1}}{\cos \delta\theta - \cos \frac{\pi}{2j+1}} \right)^2 \quad (34)$$

has variance that is bounded by π^2/N^2 , approaching that value asymptotically. In the continuous limit the phase distribution is really the Fourier transform of the input state profile. But the distribution above is not exactly the Fourier transform of a Cosine, which we would expect to be a pair of Delta functions. This is because we are forgetting the 'window' function for the state profile, $|x| < 1/2$. This 'top-hat' function would itself transform to a Sinc function and thus we may identify the above phase distribution as a convolution of two Delta functions with a Sinc function.

A further convolution with the much wider distribution of the random phase ($\Gamma^0 \gg 1/N^2$) is approximately Gaussian with increased variance $\Gamma^0 + \operatorname{var} \delta\theta$ thereby saturating the mean-squared-error bound. That it coincides with QFI bound obtained independently proves optimality of canonical phase measurements in this limit.

Analysis of Collective Relaxation/Excitation

Master equation (15) of the main text can be viewed as a finite-difference approximation to

$$\frac{1}{N} \frac{\partial}{\partial \Gamma^-} \rho = -\frac{\partial}{\partial \bar{x}} [v(x, x')\rho] + \frac{\partial^2}{\partial \bar{x}^2} [D(x, x')\rho] - \alpha(x, x')\rho \quad (35)$$

with drift, diffusion, and absorption, respectively:

$$v = -f(x)f(x'), \quad D = \frac{1}{2N} f(x)f(x'), \quad \alpha = \frac{N}{2} [f(x) - f(x')]^2, \quad (36)$$

where $f(x) = \sqrt{\frac{1}{4} - x^2}$. In the limit $N\Gamma^- \ll 1$ drift and diffusion can be neglected and the absorption suppresses off-diagonal elements as $\exp[-\mu(\frac{x+x'}{2})(\frac{x-x'}{2})^2]$, where $\mu(\bar{x}) = N^2\Gamma^- f'^2(\bar{x})$.

Larger values of relaxation lead to sudden death of precision. 'Potential' $\mu(x)$ is obtained by integrating the dephasing rate along the path given by the

drift (diffusion may be neglected). Also including dephasing and excitation processes,

$$\mu(x) = N^2\Gamma^0 + N^2\frac{\Gamma^- + \Gamma^+}{2}[\sinh s_* \cosh(s - s_*) - 1], \quad (37)$$

where $s = 2 \operatorname{artanh} 2x$ and $s_* = N\frac{\Gamma^+ - \Gamma^-}{2}$; we also use notation $\sinh x = \frac{\sinh x}{x}$. From inequality

$$1/F \geq \min_x \mu(x) = \Gamma^0 + \frac{\Gamma^- + \Gamma^+}{2} [\sinh \frac{N(\Gamma^- - \Gamma^+)}{2} - 1] \quad (38)$$

we conclude that error increases exponentially once $N(\Gamma^- - \Gamma^+) \gtrsim 1$.

Individual Decoherence: Reduced Master Equation

Although individual decoherence does not conserve total spin, master equation is invariant under qubit permutation. The density matrix transforms as a trivial representation of permutation group \mathcal{S}_N , so it must be block-diagonal corresponding to different representations corresponding to total spin S . It admits compressed representation

$$\rho = \sum_{S, m, m'} \rho_{mm'}^{(S)} \sum_{\varpi \in \Pi_S^{(N)}} \frac{|m\rangle_{\varpi} \times_{\varpi} \langle m'|}{|\Pi_S^{(N)}|} \quad (39)$$

The inner sum runs over the orthonormal basis of N -qubit representation that transforms as spin S , having dimension $|\Pi_S^{(N)}| = \frac{N!(2S+1)}{(\frac{N}{2}+S+1)!(\frac{N}{2}-S)!}$. For the purposes of computing Quantum Fisher Information we conveniently ignore the nature of ρ as a $2^N \times 2^N$ matrix and write it as a weighted sum $F = \sum_{S \leq \frac{N}{2}} w_S F^{(S)}$. Components $F^{(S)}$ are found by solving the Sylvester equation for the SLD of reduced density matrix of dimension $2S+1$.

Singling out one of the qubits, the remaining $N-1$ qubits transform as either spin $S+\frac{1}{2}$ or $S-\frac{1}{2}$ with relative weights $W_S^{\pm} = \left| \frac{\Pi_{S \pm \frac{1}{2}}^{(N-1)}}{\Pi_S^{(N)}} \right|$:

$$W_S^+ = \frac{(S+1)(N-2S)}{(2S+1)N}, \quad W_S^- = \frac{S[N+2(S+1)]}{(2S+1)N}.$$

From decomposition

$$\begin{aligned} \sum_{\varpi \in \Pi_S^{(N)}} |m\rangle_{\varpi} \times_{\varpi} \langle m'| &= \\ &\sum_{\varpi_+ \in \Pi_{S+\frac{1}{2}}^{(N-1)}} \left(C_{S_m}^{++} \left| \frac{1}{2} \right\rangle_{\varpi_+} \langle m - \frac{1}{2} |_{\varpi_+} + C_{S_m}^{-+} \left| -\frac{1}{2} \right\rangle_{\varpi_+} \langle m + \frac{1}{2} |_{\varpi_+} \right) \\ &\times \left(C_{S_{m'}}^{++} \left\langle \frac{1}{2} \right|_{\varpi_+} \langle m' - \frac{1}{2} |_{\varpi_+} + C_{S_{m'}}^{-+} \left\langle -\frac{1}{2} \right|_{\varpi_+} \langle m' + \frac{1}{2} |_{\varpi_+} \right) \\ &+ \sum_{\varpi_- \in \Pi_{S-\frac{1}{2}}^{(N-1)}} \left(C_{S_m}^{+-} \left| \frac{1}{2} \right\rangle_{\varpi_-} \langle m - \frac{1}{2} |_{\varpi_-} + C_{S_m}^{--} \left| -\frac{1}{2} \right\rangle_{\varpi_-} \langle m + \frac{1}{2} |_{\varpi_-} \right) \\ &\times \left(C_{S_{m'}}^{+-} \left\langle \frac{1}{2} \right|_{\varpi_-} \langle m' - \frac{1}{2} |_{\varpi_-} + C_{S_{m'}}^{--} \left\langle -\frac{1}{2} \right|_{\varpi_-} \langle m' + \frac{1}{2} |_{\varpi_-} \right) \end{aligned} \quad (40)$$

with Clebsch-Gordan coefficients $C_{S_m}^{\pm\pm} = \pm \sqrt{\frac{S+1 \mp m}{2(S+1)}}$, $C_{S_m}^{\pm-} = \sqrt{\frac{S \pm m}{2S}}$,

we may be able to see that Lindblad operator acting on an isolated qubit, $\mathcal{L}_k = \pi_k \rho \pi_k^\dagger - \frac{1}{2} \{ \pi_k^\dagger \pi_k, \rho \}$ (where π_k can be $s_k^z, s_k^-,$ or s_k^+) has non-zero projections on states of spin $S \pm 1$ as well as S . Differential change of the reduced density matrix may be found by taking a trace with projection operators $\sum_{\varpi} |m\rangle_{\varpi} \times_{\varpi} \langle m'|$ with $\varpi \in \Pi_{S \pm 1}^{(N)}$ or $\varpi \in \Pi_S^{(N)}$ respectively; eventual summation over all contributions ($k = 1, \dots, N$) restores the symmetric form (39).

Using this approach, reduced master equation for the combined effect of individual dephasing, relaxation and excitation can be written in compact form

$$\begin{aligned} \frac{1}{N} \frac{\partial \rho_{mm'}^{(S)}}{\partial \gamma^\sigma} &= \sum_{\substack{\tau=\pm \\ \delta=0,1}} W_{S-\tau\delta}^\tau f_{S-\tau\delta}^{\sigma\tau\delta} f_{S-\tau\delta}^{\sigma\tau\delta} m-\sigma f_{S-\tau\delta}^{\sigma\tau\delta} m'-\sigma \rho_{m-\sigma m'-\sigma}^{(S-\tau\delta)} \\ &- \rho_{mm'}^{(S)} \sum_{\substack{\tau=\pm \\ \delta=0,1}} W_S^\tau f_{S_m}^{\sigma\tau\delta} f_{S_{m'}}^{\sigma\tau\delta} - \rho_{mm'}^{(S)} \sum_{\substack{\tau=\pm \\ \delta=0,1}} W_S^\tau (f_{S_m}^{\sigma\tau\delta} - f_{S_{m'}}^{\sigma\tau\delta})^2 / 2 \end{aligned} \quad (41)$$

with coefficients $f_{S_m}^{0\tau\delta} = \left(C_{S_m}^{+\tau} C_{S+\tau\delta}^{+\tau(-1)^\delta} - C_{S_m}^{-\tau} C_{S+\tau\delta}^{-\tau(-1)^\delta} \right) / 2$ and $f_{S_m}^{\pm\tau\delta} = C_{S_m}^{\mp\tau} C_{S+\tau\delta}^{\pm\tau(-1)^\delta}$.

The integral of motion for this equation is $m - m' = \text{const}$, as expected. The third term represents ‘absorption’,

$$\alpha = \sum_{\sigma, \tau, \delta} W_S^\tau (f_{S_m}^{\sigma\tau\delta} - f_{S_{m'}}^{\sigma\tau\delta})^2 / 2,$$

$$\text{while } \begin{pmatrix} v_x \\ v_y \end{pmatrix} = \sum_{\sigma, \tau, \delta} \begin{pmatrix} \sigma \\ \tau \delta \end{pmatrix} W_S^\tau f_{S_m}^{\sigma\tau\delta} f_{S_{m'}}^{\sigma\tau\delta} \dot{\gamma}_\sigma \quad (42)$$

$$\text{and } \begin{pmatrix} D_{xx} & D_{xy} \\ D_{yx} & D_{yy} \end{pmatrix} = \frac{1}{N} \sum_{\sigma, \tau, \delta} \begin{pmatrix} \sigma^2 & \sigma\tau\delta \\ \sigma\tau\delta & \sigma\delta^2 \end{pmatrix} W_S^\tau f_{S_m}^{\sigma\tau\delta} f_{S_{m'}}^{\sigma\tau\delta} \dot{\gamma}_\sigma,$$

are ‘drift’ and ‘diffusion’ along the diagonals from the first two probability conserving terms in eqn. (41). The ‘absorption’ terms suppresses off-diagonal elements, resulting in effective rate of dephasing $\dot{\mu}$. In a continuous limit

$$\begin{aligned} \dot{\mu} &= N \frac{\dot{\gamma}^0 + \dot{\gamma}^- + \dot{\gamma}^+}{4(y^2 - x^2)}, \\ v_x &= -\left(\frac{1}{2} + x\right) \dot{\gamma}^- + \left(\frac{1}{2} - x\right) \dot{\gamma}^+, \\ v_y &= -\frac{y^2 - x^2}{2y} \dot{\gamma}^0 - \frac{y^2 + x(1+x)}{2y} \dot{\gamma}^- - \frac{y^2 - x(1-x)}{2y} \dot{\gamma}^+, \\ \text{and, less importantly, diffusion coefficients} \\ D_{xx} &= \frac{1}{N} \left[\left(\frac{1}{2} + x\right) \dot{\gamma}^- + \left(\frac{1}{2} - x\right) \dot{\gamma}^+ \right] \\ D_{xy} &= \frac{1}{N} \left[\frac{y^2 + x(1+x)}{2y} \dot{\gamma}^- - \frac{y^2 - x(1-x)}{2y} \dot{\gamma}^+ \right] \\ D_{yy} &= \frac{1}{N} \left[\frac{y^2 - x^2}{4y^2} \dot{\gamma}^0 + \left(\frac{y^2 + x^2}{4y^2} + x\right) \dot{\gamma}^- + \left(\frac{y^2 + x^2}{4y^2} - x\right) \dot{\gamma}^+ \right]. \end{aligned} \quad (43)$$

The dephasing rate $\dot{\mu}$ is integrated along the trajectory described by drift as presented in Methods.